Wang K, Pasbakhsh P, DeSilva RT, Goh KL.

A Comparative Analysis of the Reinforcing Efficiency of Silsesquioxane Nanoparticles versus Apatite Nanoparticles in Chitosan Biocomposite Fibres.

***Journal of Composites Science* 2017, 1, 9.**

DOI link to article:

https://doi.org/10.3390/jcs1010009

Date deposited:

22/01/2018

Journal of composites science

MDPI

Article

A Comparative Analysis of the Reinforcing Efficiency of Silsesquioxane Nanoparticles versus Apatite Nanoparticles in Chitosan Biocomposite Fibres

Kean Wang [1], Pooria Pasbakhsh [2], Rangika Thilan De Silva [3] and Kheng Lim Goh [4,5,*]

1 Department of Chemical Engineering, The Petroleum Institute, Abu Dhabi, P.O. Box 2533, UAE; kwang@pi.ac.ae
2 School of Engineering, Monash University Malaysia, Level 4, Building 5, Jalan Lagoon Selatan, Bandar Sunway, Selangor Darul Ehsan, Subang Jaya 47500, Malaysia; pooria.pasbakhsh@monash.edu
3 SLINTEC (Pvt) Limited, Sri Lanka Institute of Nanotechnology, Nanotechnology & Science Park, Mahenwatte, Pitipana, Homagama, Sri Lanka; rangikads@slintec.lk
4 Faculty of Science, Agriculture and Engineering, Newcastle University, Devonshire Building, Newcastle NE1 7RU, UK
5 Newcastle University Singapore, SIT Building @ Nanyang Polytechnic, 172A Ang Mo Kio Avenue 8, #05-01, Singapore 567739, Singapore
* Correspondence: kheng-lim.goh@ncl.ac.uk; Tel.: +65-9757-8847

Received: 23 June 2017; Accepted: 14 August 2017; Published: 18 August 2017

Abstract: A comparative analysis of the effects of polyhedral oligomeric silsesquioxane (POSS) and hydroxyapatite (HA) for reinforcing chitosan (CS) is given here. Wet-spun CS nanocomposite fibres, blended with HA or POSS nanoparticles, at varying concentrations ranging from 1 to 9% (*w*/*w*) were stretched until rupture to determine the mechanical properties related to the elasticity (yield strength and strain, stiffness, resilience energy) and fracture (fracture strength strain and toughness) of the composite. Two-factor analysis of variance of the data concluded that only the fracture-related properties were sensitive to interaction effects between the particle type and concentration. When particle type is considered, the stiffness and yield strength of CS/POSS fibres are higher than CS/HA fibres—the converse holds for yield strain, extensibility and fracture toughness. With regards to sensitivity to particle concentration, stiffness and yield strength reveal trending increase to a peak value (the optimal particle concentration associated with the critical aggregation) and trending decrease thereafter, with increasing particle concentration. Although fracture strength, strain at fracture and fracture toughness are also sensitive to particle concentration, no apparent trending increase/decrease is sustained over the particle concentration range investigated here. This simple study provides further understanding into the mechanics of particle-reinforced composites—the insights derived here concerning the optimized mechanical properties of chitosan composite fibre may be further developed to permit us to tune the mechanical properties to suit the biomedical engineering application.

Keywords: hydroxyapatite; polyhedral oligomeric silsesquioxanes; elasticity; fracture; particle shape; particle concentration; Weibull model

1. Introduction

To overcome the limitations of biopolymers, such as low stiffness and strength, and to enable these materials to have wide applicability, inorganic particulate fillers are often blended with the biopolymer to form a composite material that possesses enhanced stiffness and strength [1–3]. This study is concerned with chitosan (CS) biopolymer, a linear polysaccharide that can be derived from the alkaline *N*-deacetylation of chitin [4,5]. Chitin is the main structural component

of the shells of crustaceans, the exoskeletons of insects and the cell walls of fungi [4–8]. CS polysaccharide is a copolymer comprising β-(1-4)-2-amino-D-glucose (deacetylated unit) and β-(1-4)-2-acetamido-D-glucose (acetylated unit) [4,5]. When the amount of deacetylated unit is higher than 50%, the resultant compound is known as chitosan, otherwise it is known as chitin [4,5]. CS has been a subject of great interest owing to its biocompatibility-related advantages, notably anti-clotting, biodegradability [4,9], antimicrobial and low toxicity (even in blends) [10–12]. Thus, it can be used for medical products such as bandages and implants, or grafted with compounds to yield chelating agents that can be used in water filters [10–12].

A key concern about employing CS in a number of these applications is the low mechanical strength and stiffness [5]. The low values of the mechanical properties of CS limit the applicability for tissue engineering, particularly as implants for soft connective tissues. According to Di Martino et al. [13] and the references therein, the hydrated CS has tensile moduli of 0.1–0.5 MPa (porous membrane) but 5–7 MPa (non-porous membrane). Albanna et al. [14] reported that dehydrated CS fibres have tensile moduli of 2–10 MPa. CS membranes appear to possess higher stiffness; tensile modulus for CS (solution-casted) membranes was found to be in the range of 400–800 MPa [15,16]. Electrospun CS membranes could exhibit a lower tensile modulus of about 300 MPa [17]. CS (solution-casted) membranes have an extensibility (i.e., maximum strain to rupture) of about 0.3 [16]; the extensibility of electrospun membranes varied from 0.3 [13,17] to 1.0 [13]; this variability depends on the pore size and pore orientation [13]. Albanna et al. [14] reported that CS fibres have extensibility values ranging from 0.10 to 0.25. With regards to tensile strength, porous CS structures were found in the range of 30–60 kPa (Di Martino et al. [13] and therein). Liu et al. [15] reported that the CS (solution-casted) membrane has a tensile strength of about 20 MPa. Albanna et al. [14] reported that the CS fibres have tensile strength of 0.4–1.4 MPa. Overall, the strength and modulus of CS materials are much lower than those of soft connective tissue [18], such as skin [19], tendons [20–22] and ligaments [23,24].

To this end, attempts have been carried out to 'tune' the mechanical properties of the CS material by blending with nanoparticles made from, e.g., hydroxyapatite (HA) [25] or silsesquioxane [26,27]. The physical and chemical properties of blends of CS containing HA particles have been well investigated [25,28–34], and CS/HA composites have been proposed for making implantable scaffolds to achieve the desired magnitude of the respective mechanical properties by 'tuning' the HA concentration [30]. The optimised composite is then expected to be useful for influencing the lineage of scaffold-seeded stem cells to generate an extracellular matrix that is compatible with the microenvironment of the host tissue, as well as provide structural support to the host tissue [14]. Blends of CS containing silsesquioxane, namely polyhedral oligomeric silsesquioxane (POSS) particles, have attracted some investigations [26,35,36] and may be a potential alternative to CS/HA. POSSs are compounds having a polyhedral siloxane cage, with the formula $(RSiO_{1.5})_n$ (where n = 6, 8, 10, 12 and R = H or organic substituents) [27]. The most common molecular formula of POSSs is n = 8; the overall size of the molecule is about 1–3 nm [27]. The key practical advantages of using POSS for blending with polymers are summarized as follows (Reno et al. [37], Blanco et al. [27] and therein). (A) POSS are organosilica three-dimensional, cubic building blocks containing an inorganic inner siloxane core that can be chemically modified at each of the eight corners of the POSS unit. (B) POSS featuring reactive organic groups can be employed as cross-link agents for the preparation of hybrid hydrogel samples. (C) POSS molecules are physically dispersed through weak interactions with the polymeric matrix. This latter approach has important advantages in terms of low cost and synthesis time. (D) It is noted that a homogeneous dispersion of POSS in the matrix may be easily obtained [38–41]. However, only a limited amount of work has been carried out on CS/POSS blends compared to CS/HA blends. For structural applications, the single most important question that has yet to be addressed adequately is how do the magnitudes of the mechanical properties of CS/POSS compare to CS/HA, all things being equal?

To this end, an in-depth analysis of POSS and HA particles for reinforcing CS composite materials has been carried out. Here, both CS/POSS and CS/HA fibres were synthesized by a wet spinning method. The analysis addresses the effects of the particle types (i.e., POSS or HA) and concentration as well as the interaction between the two factors on CS composite. The arguments that underpin the effects of particle concentrations have been investigated for the respective particles and reported in the literature [25,26]. However, most of the reports involve experiments with particle concentration as a single treatment and the experimental conditions are not necessarily the same. Thus, from the material design perspective, optimisation-related arguments concerning the effects of particle types and concentration and the interaction between the two on CS composite seem to be much less well established. To clarify which types of particle would exhibit advantages over the other, as well as to broaden our understanding of the underlying mechanisms of nanoparticulates for reinforcing chitosan composite material, this study investigates the effects of particle type, at varying particle concentrations, on the chitosan composite elasticity and fracture. We hypothesize that the underlying shape of the respective particle type and agglomeration, as well as the interaction between the two factors, influences the mechanical properties of the chitosan composite. A statistical approach, i.e., the two-factor analysis of variance (ANOVA), was used to evaluate the mechanical data and determine the influence of particle type and concentration on the mechanical properties of these CS composite fibres. The mechanical reliability of the nanocomposite was analysed using the Weibull model.

2. Materials and Methods

2.1. Preparation of Chitosan Fibres

The POSS used in this study refers to aminopropylphenyl POSS (AM0272; Hybrid Plastic Inc., Hattiesburg, MS, USA). HA was obtained from Sigma-Aldrich, St. Louis, MO, USA. The CS (85% deacetylated) used in the study were also purchased from Sigma-Aldrich.

CS-based solutions were prepared at the predetermined particle concentrations of the respective HA and POSS, following a protocol that had been reported in a previous study for CS/POSS fibres [26]. Here, a 1.5% w/v concentration of CS to acetic acid was prepared (NB: 1% w/v is equivalent to 0.01 g/mL), and 10 mL of 1% concentration acetic acid was used as a solvent to dissolved 0.15 g of CS. The solution was then stirred at a constant rate of 700 rpm at room temperature. HA and POSS of concentrations 1% (w/w), 3% (w/w), 5% (w/w), 7% (w/w) and 9% (w/w) were added to the CS. (These concentrations corresponded to the masses of 0.0015 g, 0.0045 g, 0.0075 g, 0.0105 g, and 0.0135 g, respectively.) For the CS/POSS blending process, first of all the CS solution was stirred at a constant rate of 700 rpm for 4 h to ensure that the CS was completely dissolved. Consequently, after the POSS was added, the blend was stirred at a constant rate of 700 rpm at room temperature for 18 h before it was introduced into the wet spinning device. Similary, for the CS/HA blending process, the CS solution was stirred at constant rate of 700 rpm for 4 h before the HA was added. After the HA was added, in order to avoid prolonged exposure of HA in an acidic pH environment, the CS/HA blend was stirred at constant rate of 700 rpm for 2 h before it was subjected to the wet spinning process.

CS-based fibres were processed by a wet spinning method, outlined as follows. Figure 1A illustrates a setup of the apparatus for this method. Overall, the process involved (A) extruding the CS solution (containing the particles), through a spinneret, into a coagulation bath containing a non-solvent where the precipitation of the CS-based fibres occurred [25,26,42]; (B) washing the fibres to remove coagulant remains; and (C) winding up the fibres using a bobbin [25,26,42]. The dope (i.e., the blend solution) was made to flow through a syringe pump set at rate 5 mL /min. This dope was then pumped through an epoxy-cured silicone tube into a bath of 1 M of NaOH (i.e., a coagulation bath). Before starting to pump the dope through the system, the tube was first used to deliver a 1 M NaOH solution at a rate of 5 mL/min. Then, the dope was mixed with the coagulant solution at a junction; it was in this bath that the CS would precipitate into a fibre-like form. The CS-based fibres were left in the coagulant solution for 15 min (Figure 1B); thereafter they were removed from the coagulant

solution and rinsed with deionised water. Removing the fibres from the solution by winding them around a cylindrical bobbin helped to laterally deform the fibre to achieve a ribbon-like cross section (inset in Figure 1B). The result of the ribbon-like shape resembled a near-triangular cross section when viewed under a field-emission scanning electron microscope (FE-SEM, JEOL JSM-6390LA, JEOL Ltd., Tokyo, Japan) (results not shown).

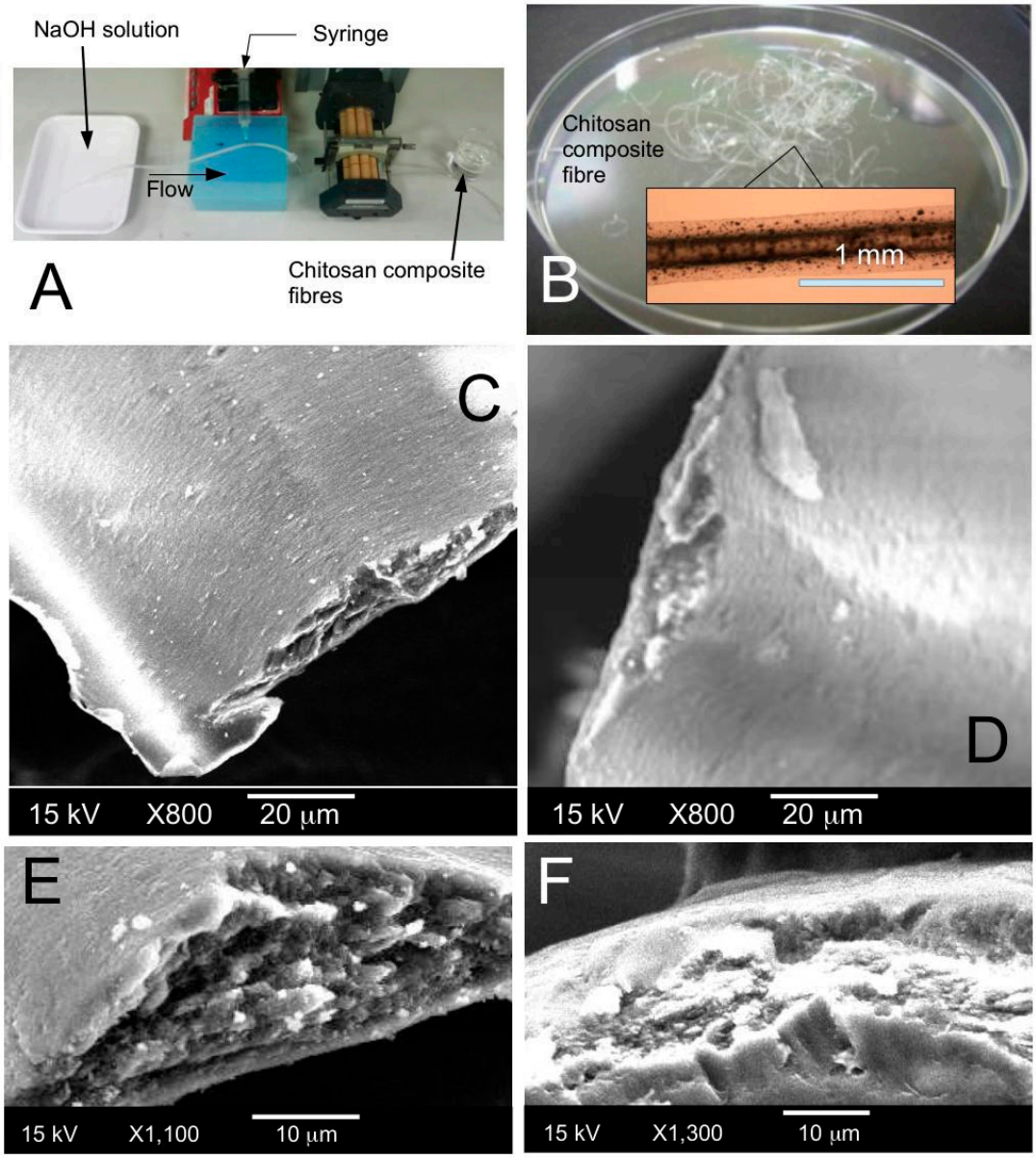

Figure 1. The chitosan composite fibres. (**A**) Set-up of the wet spinning process; (**B**) wet-spun chitosan-based fibres in a petri dish (inset shows a micrograph of the fibre taken using an optical microscope). Low magnification scanning electron micrographs (SEMs) of the cross-section of chitosan fibre reinforced by hydroxyapatite (HA) (**C**) and polyhedral oligomeric silsesquioxane (POSS) (**D**); panels (**E**) and (**F**) show the SEMs of the respective fibres at higher magnification.

2.2. Tensile Testing

The fibres were tested to rupture using a custom-built micromechanical tester [26]. Ten tensile specimens were prepared—according to a method described in previous study [26]—for each of the different combinations of particle type and concentration. Before the test began, the gauge length

(i.e., grip-to-grip distance) and cross-sectional area (identified with the area of a triangle) of each fibre specimen were recorded. Specimens were stretched to rupture at a displacement rate of 0.067 mm/s. The fracture morphology of the microstructure was examined using a FE-SEM. The force versus displacement data for the respective specimen were evaluated to derive the stress–strain curve. Here, stress was determined from the force divided by the cross-sectional area of the fibre; strain was determined from the ratio of the fibre displacement to the gauge length. Following the definition based on previous reports [26], the yield point (which is identified by the point of inflexion between the origin and the maximum stress point on the stress–strain curve) was used to determine the yield strength (σ_Y), yield strain (ε_Y), stiffness (E), and strain energy density to yielding (u_Y), otherwise known as resilience energy). The maximum stress point was identified to correspond to the fracture strength (σ_U) and the fracture strain (ε_U, otherwise known as extensibility); the strain energy density to fracture (u_F, otherwise known as fracture toughness) was determined up to this point [26,43].

2.3. Statistical Analysis

Two-factor ANOVA was primarily used to test our hypotheses (Section 1), i.e., that the particle type and concentration have significant effects on the respective mechanical properties and that interactions occur between the two factors, at an alpha level of 0.05. When interaction effects caused a masking of the results (such as in the case of CS/HA versus CS/POSS), a Student's t-test was used to analyse for differences at the respective levels. A test was regarded as significant when p value < 0.05.

2.4. Weibull Model

To analyse the mechanical reliability of the composite fibres, the Weibull model was applied to evaluate the mechanical data. Let β and σ_0 represent the Weibull modulus and the characteristic strength, respectively. Adapting the method for fracture analysis (probabilistic approach) from a previous study on CS/HA with respect to particle concentration versus crystallisation temperature [34], according to Weibull's empirical law [44], the cumulative distribution function (C) of the yield/fracture stress of the CS composite fibre, σ, for determining failure due to flaws is given by $C(\sigma) = 1 - \exp(-[\sigma/\sigma_0]^{\beta})$.

To apply the Weibull law to the probabilistic analysis of the yield/fracture of the CS composite fibre, first one notes that β quantifies the variability of σ; low β values correspond to high variability and vice versa [44]. Second, one notes that σ_0 is the stress value at which 63% of the fibres have yielded/fractured [44]. Normally, for the convenience of analysis the C function is replaced by the reliability function, R (= 1 − C), which describes the proportion of the population of specimens sampled that survive at fracture stress σ. Thus the expression for R is given by

$$R(\sigma) = \exp(-\{\sigma/\sigma_0\}^{\beta}). \quad (1)$$

Additionally, the median rank position,

$$\mathrm{M} = \{i - 0.3\}\{n + 0.4\} - 1, \quad (2)$$

where n represents the size of the treatment group and i is the position of the corresponding σ, is numerically identified with the R. It then follows that M is used to compute the R as an intermediate step in the Weibull analysis.

We have adopted the following practical approach to evaluate β and σ_0 for the different treatment groups, namely CS/HA versus CS/POSS and particle concentration levels. First, we determined the M for each experimentally derived value of σ (i.e., σ_Y or σ_U). This was carried out by ranking the magnitudes of the σ (i.e., σ_Y or σ_U) in ascending magnitude. The corresponding estimates of M were evaluated using Equation (2). Second, we fitted straight lines to the so-called Weibull plot of $\log(\log(1/\{1 - \mathrm{M}(\sigma)\}))$ versus $\log(\sigma)$ for each group. Finally, the value of β was identified with

the slope of the respective straight lines; the value of σ_0 was found after equating $-\beta\log(\sigma_0)$ to the y-intercept of the straight line.

3. Results

3.1. Fracture Morphology

The overall fracture morphologies for the CS/HA and CS/POSS fibres (Figure 1) appear somewhat similar. The fractured planes are near-perpendicular to the axis of the fibre, suggesting that the fibres fail by brittle fracture. All fibres exhibit similar fissures and projection features. These could be attributed to a combination of the following modes of failure: (A) detachment (i.e., pullout) of the HA or POSS particles from the chitosan matrix (inter-granular failure); (B) fracture of the HA or POSS particles (trans-granular failure). POSS compounds are in the form of nanoparticles; in principle these could be observable in the fibres using a SEM with high magnification. So far, these are the best images that one could derive from SEM imaging. Here we also noted that the images reported elsewhere by other researchers reveals POSS in large particulates on the order of 1 μm, when blended in a chitin matrix [8]. Note that the ribbon-like profile of the fibre cross section was the result of lateral compressive forces that were generated by the extruded fibre by winding around a bobbin during the wet spinning process. Of note, the ribbon-like profile could present an advantage as it possesses a greater surface area for cell adhesion. Additionally, if the fibres could be laid down in the form of a mesh, the 'pores', i.e., the space between the fibres, need to be sufficiently large for cells to migrate into the mesh, where they eventually become bound to the surfaces in the scaffold. Nevertheless, the design of a scaffold mesh made from such CS fibres is promising but further work is required to optimise the fibre surface area per unit volume (A_{SA}) and pore size (D_{pore}) [45,46].

We have not attempted to mesh our fibres as the main focus is on the properties of the single fibre. In our samples, the ribbon-like profile provides a broad surface of about 2pi × 40/2 (μm) = 126 μm. To this end, we could expect that the pore sizes are on the order of 100 μm or more. Fibroblasts are on the order of magnitude of 40–60 μm [47]. Osteoblasts and chondrocytes are on the order of 10 μm [48]. More importantly, the sizes of these cells are consistent with the dimensions of the fibre thickness, as well as the predicted size of the pore.

If a scaffold (meshed) is to be fabricated from CS/HA or CS/POSS fibres, the first issue to address is how to lay down the fibres with regards to having a fibre orientation predominated by primary fibres in one direction (to provide certainty in strength and stiffness) and randomly oriented secondary fibres. What then is the mechanical property of this configuration? It turns out that for such a design, the strength of the mesh (which is related to the probability of rupturing of a fibre section) is dictated by the Weibull distribution of stresses (Section 3.4). The overall tensile strength of the mesh (when gripped at both extreme ends to stretch to rupture) would be lower than that of a single fibre [49].

3.2. Effects of Particle Type and Concentration on the Elastic Properties

To begin, we have found significant differences ($p < 0.05$) for the respective E (Figure 2A) and σ_Y (Figure 2B) versus particle concentration and particle type. No significant interaction between the two factors is observed ($p > 0.05$). For the main effects of particle type, the mean E and σ_Y of the CS/POSS fibres are higher than those of the CS/HA fibres. As for the main effects of particle concentration, the mean E and σ_Y are highest at 3% (w/w) and lowest at 9% (w/w) particle concentration. It can be concluded that (A) the CS/POSS fibres are stiffer and have higher yield strength than those of CS/HA; and (B) an optimal particle concentration that leads to the highest stiffness and yield strength occurs at 3% (w/w).

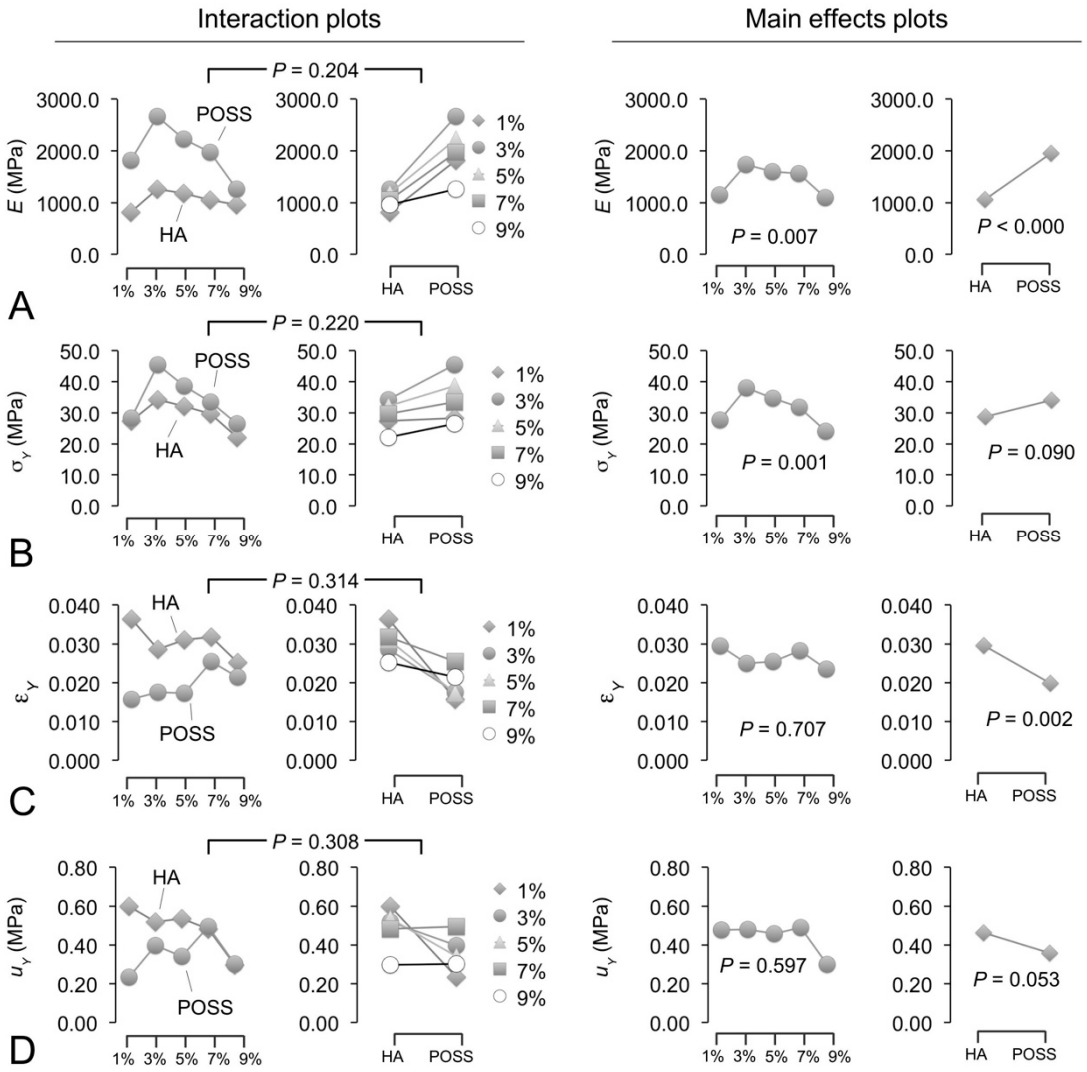

Figure 2. Interaction (**left panel**) and main effects (**right panel**) of particle concentration (% w/w) and particle type on the elasticity-related properties of chitosan-based fibres reinforced by hydroxyapatite (HA) versus polyhedral oligomeric silsesquioxane (POSS) particles. Symbols: (**A**) E, elastic modulus; (**B**) σ_Y, yield stress; (**C**) ε_Y, yield strain; (**D**) u_Y, strain energy density for resilience.

The p value for the effects of particle type on ε_Y is small ($p = 0.002$), revealing strong evidence of the influence of particle type on ε_Y (Figure 2C). However, this is not the case for ε_Y versus particle concentration ($p = 0.707$). Since the p value for the interaction between particle concentration and particle type is much greater than 0.05 (interaction $p = 0.314$), this suggests that there is no evidence of an interaction between the factors. We conclude that ε_Y is sensitive to variation in particle type but not to particle concentration. In considering the main effects of particle type, it is observed that the mean ε_Y from the CS/HA fibre is higher than that of the CS/POSS fibre. We conclude that CS/HA fibres are more deformable, i.e., they yield at larger strains than CS/POSS fibres.

As for u_Y, we note that the p values for particle type ($p = 0.053$) and particle concentration ($p = 0.597$) are both greater than 0.05 (although the former may be regarded as marginal). Thus, there is no evidence that u_Y is sensitive to particle type and concentration (Figure 2D). The p value for the interaction is much greater than 0.05 ($p = 0.308$), showing that there is no evidence of an interaction between the factors. Altogether, this suggests that u_Y is not sensitive to variations in particle concentration and type.

3.3. Effects of Particle Type and Concentration on Fracture Properties

With regards to σ_U, the ANOVA results (Figure 3B) reveal a significant interaction between particle type and particle concentration ($p < 0.001$). Thus the main effects may not be interpreted independently of one another. Figure 3A shows that σ_U is sensitive to variations in particle concentration ($p < 0.001$) but not particle type ($p = 0.216$). It appears that the optimal particle concentration occurs at 3% or 7% (w/w) depending on the particle type. The main effects due to particle type could be masked by interaction effects and warrant further analysis. To address the effects arising from interaction, a two-sample t-test was conducted to investigate the differences in σ_U between the CS/HA and CS/POSS at the respective particle concentration levels. The results of the t-test reveal no significant difference in σ_U between the CS/HA and CS/POSS for all levels of particle concentration except at 7% (w/w) ($p < 0.001$)—the mean σ_U of the CS/HA fibres is smaller than that of CS/POSS fibres at 7% (w/w).

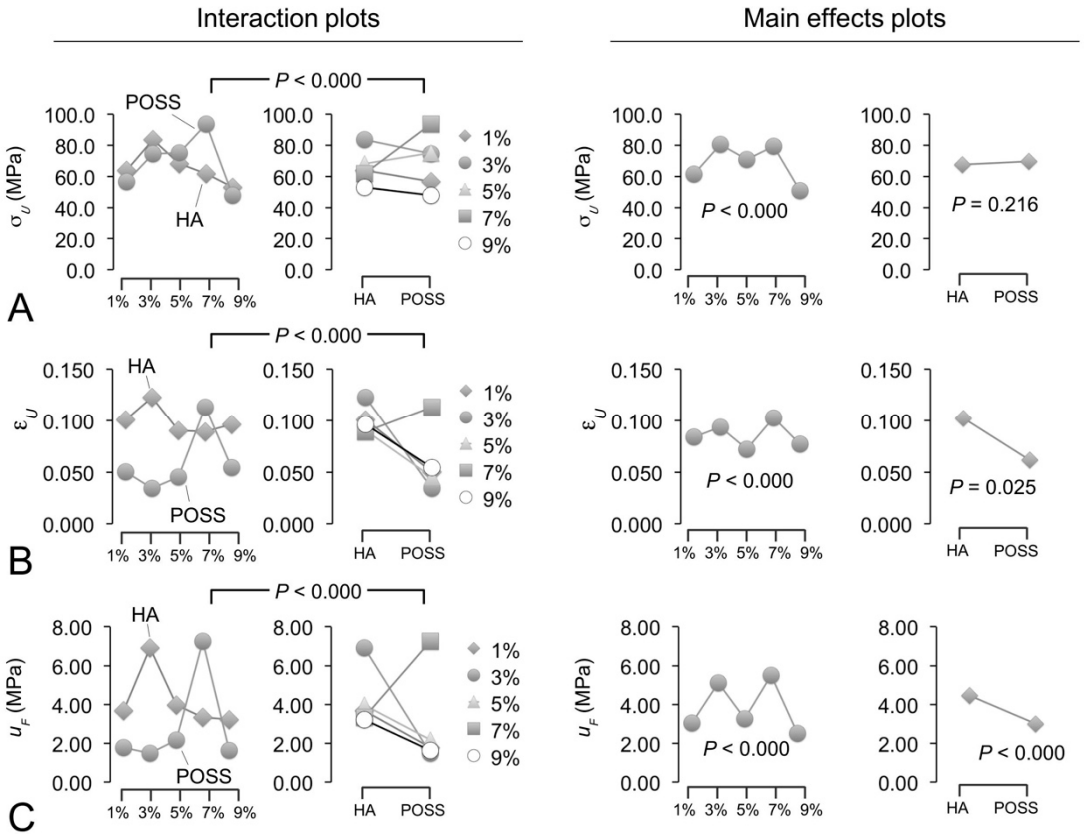

Figure 3. Interaction plots (**left panel**) and main effects (**right panel**) plots of particle concentration (% w/w) and particle type on the fracture-related properties of chitosan-based fibres reinforced by hydroxyapatite (HA) versus polyhedral oligomeric silsesquioxane (POSS) nanoparticles. Symbols: (**A**) σ_U, fracture strength; (**B**) ε_U, extensibility; (**C**) u_F, strain energy density to fracture.

With regards to ε_U, a significant interaction between particle concentration and type occurs ($p < 0.001$). Thus the main effects may not be interpreted independently of one another. Here, significant differences are observed for ε_U versus particle type ($p < 0.001$) and particle concentration ($p = 0.025$) (Figure 3B)—the ε_U is sensitive to variations in particle type and particle concentration but the effects of particle type on ε_U is modified by particle concentration and vice versa. We conclude that (1) the mean ε_U from the CS/HA fibre is higher than that of the CS/POSS fibre (except at 7% w/w, where both result in similar magnitudes of ε_U); and (2) the optimal particle concentration resulting in the highest ε_U occurs at 7% (w/w).

Finally, with regards to u_F, the p value for the interaction between particle type and concentration is very small ($p < 0.001$), showing that there is evidence of an interaction between the two factors. Thus, the main effects of particle type and particle concentration on u_F may not be interpreted independently of one another. Nevertheless, significant differences are observed for u_F versus particle type ($p = 0.001$) and particle concentration ($p < 0.001$) (Figure 3C). In considering the main effects of particle type, it is observed that the mean u_F from the CS/HA fibres is about 40% higher than that of the CS/POSS fibres. For the consideration of the main effects of particle concentration, the mean u_F appear to peak at 3 or 7% (w/w), depending on the particle type. We conclude that the optimal particle concentration, corresponding to maximum u_F occurs at 3 and 7% (w/w) for HA- and CS/POSS fibres, respectively.

3.4. Mechanical Reliability

Table 1 lists the values of the Weibull modulus, β, and the characteristic strength, σ_0, of the CS composite fibre reinforced by HA and POSS nanoparticles, associated with the yield strength and fracture strength parameters. Inspection of the values of β in the table reveals the following trends. With regards to the yielding of CS/HA composite fibre, it is observed that β increases with the increase in POSS concentration, peaks at 7% w/w, and decreases somewhat thereafter. As for the yielding of the CS/POSS composite fibre, it is observed that β increases rapidly with an increase in POSS and peaks at 3% w/w (as compared to 7% w/w for the case of CS/HA), followed by a decrease in β, with increasing POSS concentration. On the other hand, with regards to the fracture of the CS fibre, the β from both CS/HA and CS/POSS appears to fluctuate with increasing particle concentration, and no appreciable trend is observed.

Table 1. Analysis of the Weibull modulus, β, and the characteristic strength, σ_0, of chitosan (CS) fibres reinforced by hydroxyapatite (HA) and polyhedral oligomeric silsesquioxane (POSS) nanoparticles.

Particle Concentration % *w/w*	CS/HA				CS/POSS			
	Yield Strength		Fracture Strength		Yield Strength		Fracture Strength	
	β (MPa)	σ_0 (MPa)	β (MPa)	σ_0 (MPa)	β (MPa)	σ_0 (MPa)	β (MPa)	σ_0 (MPa)
1	4.58	37.53	7.21	69.43	2.40	31.76	13.00	58.96
3	4.80	38.31	12.90	86.26	7.90	48.11	4.70	85.35
5	4.90	35.57	9.80	70.46	4.40	42.52	3.50	83.81
7	5.30	32.80	15.80	62.76	2.60	37.17	13.30	97.41
9	3.70	24.27	7.80	55.30	2.50	32.46	9.40	50.68

Inspection of the values of σ_0 in the table reveals the following trends. With regards to the yielding of CS composite fibre, both CS/HA and CS/POSS show that σ_0 increases with an increase in the particle concentration, peaks at 3% w/w, and decreases somewhat thereafter. On the other hand, as for the fracture of the CS/HA fibre, σ_0 increases with increasing HA concentration, peaks at 3% w/w, and decreases thereafter. In contrast, for the CS/POSS fibre, σ_0 increases with increasing POSS concentration, peaks at 7% w/w, and decreases thereafter.

Figure 4 shows plots of R versus σ for the CS/HA and CS/POSS fibres corresponding to the cases of yielding and fracture. These plots illustrate the sensitivity of the reliability to the β and σ_0 parameters at the respective levels of particle concentration and type. With the exceptions of the yielding of CS/POSS at 1%, 7% and 9% w/w and the fracture of CS/POSS fibre at 3% and 5% w/w, the form (i.e., parameterized by β) of the curves corresponding to CS/HA and CS/POSS features a very narrow spread of strength variability, for the respective case of yielding and fracture. The scatter of the curves deserves some attention. With regards to the respective HA and POSS particles, over the range of particle concentration considered here, the curves for the yielded CS fibre (Figure 4A (C)) are less scattered compared to those of fractured CS fibres (Figure 4B (D)). The implications of these results are discussed in Section 4.2.

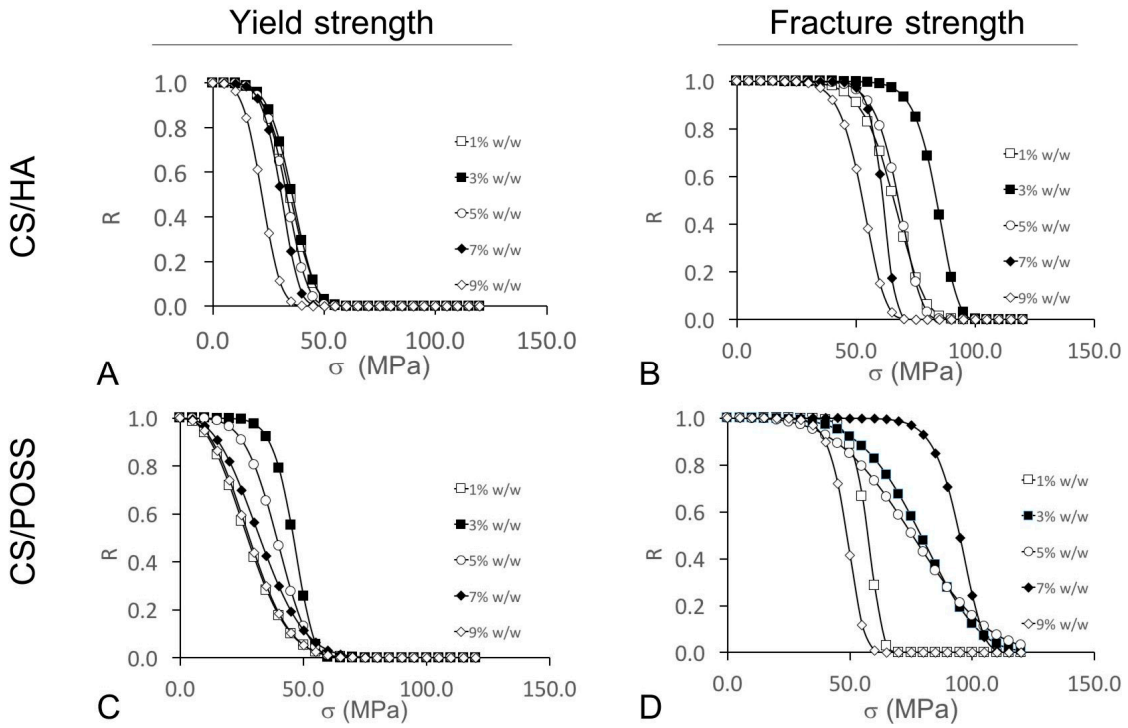

Figure 4. Plot of reliability function, R (a dimensionless quantity), versus stress (σ, MPa) in the chitosan-based composite fibre, reinforced by hydroxyapatite (HA), for the case of (**A**) yield strength and (**B**) fracture strength, and polyhedral oligomeric silsesquioxane (POSS), for the case of (**C**) yield strength and (**D**) fracture strength, in the presence of varying particle concentrations (% *w*/*w*). Note: σ_0 and β represent the characteristic strength and the Weibull modulus, respectively.

4. Discussion

4.1. Study Findings

In this study, both CS/POSS and CS/HA fibres were synthesized by a wet spinning method, with varying particle concentrations from 1% to 9% (*w*/*w*). Wet spinning is a simple and effective method that involves a combination of rheological and diffusional mechanisms to synthesize fibres with controlled thickness [25,26,50,51]. Methods such as melt spinning are not feasible as the CS polymers degrade upon heating [25,51]. It is important to note that the wet spinning method can produce useful fibres because the flow action during extrusion helps to align both the CS polymer molecules and the nanoparticles in the direction of the fibre axis, thus contributing to axial reinforcement [26]. From the perspective of tissue engineering scaffolds, it makes sense to synthesize CS fibres of micrometre thickness for several reasons, namely they can lead to large surface area for cell attachment as well as enhanced interconnected pore architecture that provides pathways for the diffusion of gases, transportation of nutrients, and migration of cells [11,52–54].

According to some reports, isolated particles of HA and POSS are physically distinguished by their shapes: HA are generally described as having a needle-like (generally rods or with straight-taper ends) profile [55,56] while POSS particles may be described as having globular profiles [57]. While these descriptions are not based on a detailed analysis of the particle shapes, the precise form of these particles (at least for HA particles [25]) is expected to depend on the precipitation temperature, which ranges from ambient [58,59] to 40 °C [29,50,51,60]. More importantly, both particle types provide a unique perspective to study the effects of non-uniform cylindrical profiles of a nanoparticle-reinforced composite and its mechanical properties [30]. Although the exact forms of these particles in the composite are not observable, predictions from finite element models of composites reinforced by

ellipsoidal particles and needle-like particles with straight tapered ends reveal that the stress uptake in these particles is somewhat evenly distributed throughout during elastic loading [61]. On the other hand, uniform cylindrical (i.e., rod shape) particle-reinforced composites feature a peak stress at the particle centre; the stress decreases non-linearly to zero at the particle ends [62]. In principle, the non-uniform cylindrical particles are less likely to break owing to lower stress concentrations, and hence are more effective than uniform cylindrical ones for composite reinforcement [62,63] Nonetheless, these predictions have yet to be supported by experimental results.

There are some reports of 'hybrid' composites, notably from the study based on computer modelling of a composite comprising (i.e., non-fibre-like) particles and fibres blended in polymer composites [64], and banana/sisal fibres blended in epoxy resin [65]. Of note, the mechanical properties of a banana/sisal fibre-reinforced epoxy resin composite have been evaluated based on the rule-of-mixture for hybrid composites [49]. However, to the best of our knowledge, there is no study hybridizing chitosan by blending with POSS and HA particles. This would be an interesting study with regards to optimising the chitosan composite mechanical properties.

In principle, the magnitudes of the mechanical properties (such as strength and stiffness) are expected to increase linearly with particle concentration in good order-of-magnitude agreement with the simple rule-of-mixture for strength and stiffness [30]. In practice, composites reinforced by nanoparticles (such as those shown in this study for the CS/HA and CS/POSS, and in other studies, namely (A) SiO_2 particles reinforcing polyimide [1], (B) $BaSO_4$ particles reinforcing polypropylene [66], and (C) carbon nanotubes reinforcing ceramic [67]) do not follow the rule-of-mixture at large particle concentration levels. In fact, there exists a particle concentration level beyond which a further increase in particle concentration leads to a diminution in the mechanical properties. This effect is often attributed to the extensive agglomeration of nanoparticles beyond the optimal particle concentration [1,30,68]. Further discussion of the underlying causes of agglomeration is found in Section 4.2. Nevertheless, the low particle concentration is a cause for concern as it severely constrains the tunability of the mechanical properties of the composite to a narrow range of particle concentrations. Interestingly, the peak value of different mechanical parameters appears to differ. For instance, the highest stiffness occurs at 3% *w*/*w* but the highest fracture strength occurs at 7% *w*/*w*. This means that if the material designer is required to design the CS composite fibre for high fracture strength, the trade-off would be lower stiffness.

An interesting study has been carried out by Aranaz et al. [69] to investigate the type of calcium phosphate formed in the CSCaP monoliths. There are two key findings according to this study [69]. (A) Calcined samples showed a pattern similar to enamel (highly crystalline apatite mineral, ca. 96 wt. %), and non-calcined samples showed a pattern similar to dentin (partially amorphous apatite, which also contains an organic matrix and water). (B) The amount of calcium phosphate in the CSCaP composites can significantly influence the efficacy of cell proliferation: it is found that higher calcium phosphate content in the composite enhances cell attachment and proliferation and vice versa. With regards to our CS fibres, it would be interesting as part of future work to assess the extent of the crystallinity in the CS fibres. This could come together with plans for cell studies. With regards to cell studies, one key area of interest is in developing a consistent technique to lay down the fibres into a mesh. The study of osteoblast and chondrocyte cells in tissue engineering with regards to cell adhesion, spreading, and viability is an ongoing interest [48]. With regards to our CS fibres, one future work of interest would be to investigate how these cells respond to the fibrous mesh when they are seeded into the mesh. A method will be developed to enable consistency in the seeding process using an in-house developed automated cell dispensing machine; such a machine may be modified from an open-sourced 3D printer [70].

Although the mechanical properties of the CS/HA composite are well established and a few reports have been published on the CS/POSS composite, most reports have been concerned with singly applied treatments. In other words, these experiments have attempted to investigate only one synthesis parameter, notably the effects of particle concentration [25,26]. Here, the results from the

two-factor ANOVA reveal that particle concentration and particle type do interact. With regards to the sensitivity of the mechanical properties of CS composite fibre to particle concentration and particle type, the findings are listed as follows: (A) Only the fracture-related mechanical parameters, i.e., σ_U, ε_U and u_F, are sensitive to interaction effects. Since these parameters are also sensitive to particle concentration and type, the trending variation of the values of each of these parameters with varying particle concentration (type) depends on particle type (concentration). As for the elasticity-related parameters (i.e., E, σ_Y, ε_Y and u_Y), the results suggest that the main effects (where applicable) of particle concentration and particle type on these parameters may be interpreted independently of one another. (B) With regards to effects from particle type, by and large the σ_Y and E of CS/POSS fibres are higher than CS/HA fibres but CS/HA fibres possess higher ε_Y, ε_U and u_F than CS/POSS fibres. This suggests that CS/POSS fibres are stronger and stiffer than CS/HA fibres but CS/HA fibres are not only less brittle but also tougher than CS/POSS fibres. The u_Y is not sensitive to particle type. (C) With regards to effects from particle concentration, only E and σ_Y reveal a clear trending increase up to an optimal particle concentration; thereafter a trending decrease occurs. The optimal particle concentration differs for different mechanical properties. In particular, E and σ_Y peak at 3% (w/w). The ε_Y and u_Y are not sensitive to particle concentration. Interestingly, due to the presence of interaction between the particle concentration and particle type, σ_U, ε_U and u_F peak at 3% or 7% (w/w), depending on particle type.

The E, u_Y and u_F may be regarded as 'derived parameters', defined in terms of both stress and strain components. By considering the results from the main effect study (Sections 3.2 and 3.3), we infer that (A) the stress component predominates in E as demonstrated by σ_Y; (B) the strain component (from initial loading until ε_U) predominates in u_F, as demonstrated by ε_Y. While further discussion concerning the basis for the absence of sensitivity of the u_Y of chitosan composite fibre to nanoparticles of HA and POSS could be valuable, the answer is not as clear-cut as we might wish. Nevertheless, the underpinning arguments suggest that the mechanics of nanoparticles of HA for modulating the stress and strain (by directing low stress uptake at high strains) is in direct contrast to that of POSS (by directing high stress uptake at low strains). However, in either case, these lead to similar results arising from a similar amount of strain energy absorbed per unit volume (i.e., u_Y) causing yielding in the fibre.

4.2. Design for Reliability

It is possible that defects in the CS fibre may originate from agglomerates of HA or POSS, as well as localised non-uniform dispersion of the respective particles within the CS fibre—these defects then act as stress intensifiers. Failure in the fibre may begin at these stress intensifier site as the load on the fibre increases; yielding occurs when chemical bonds within the defects are partially disrupted but rupture, i.e., formation of new crack surfaces, occurs when all the chemical bonds at a particular site are dissociated.

The reliability predictions reveal that the CS/HA composite fibres have more consistent (in other words, narrower spread of σ values) yield and fracture strengths as compared to CS/POSS composite fibres. Thus this could be attributed to two factors: (A) the agglomeration of particles and (B) the directionality of the particles. The agglomerates could compromise the mechanical properties of the composite fibre. As these agglomerates are weakly bonded together, the dissociation of these agglomerates could in turn contribute to increased unpredictability in the yield and fracture strength of the CS/POSS fibre. Additionally, as the POSS particles are described as having globular profiles (Section 4.1), this means that in some POSS particles the long axis may be comparable in length to the short axis. Thus, during the processing of the CS/POSS fibre, as the POSS particles flow though the tube and spinneret, the flow effect may not be sufficient to cause the long axis of all POSS particles to point in the direction of the fibre axis. Consequently, the directionality of the POSS particles is less defined than that of HA particles, which are described as having needle-like profiles. The directionality of the particulates plays an important role in determining the mechanical properties of the CS composite fibre. According to the principles of particle-reinforced composites, a composite that contains well-aligned particles will have higher strength when an external load is applied in the

direction of these particles [26]. For composites that contain particles that are not well aligned, only a proportion of the particles that are aligned in the direction of the applied load would be able to provide effective reinforcement by taking up stress from the matrix [26].

The possible contribution of particle agglomeration to the decrease in the magnitude of the respective mechanical parameters, at high particle concentration levels, is an issue of great concern [68]. As these agglomerates are weakly bonded, individual agglomerates dissociate easily into smaller particles under high load—smaller particles, with shorter length, may be less effective at taking up high stress. Exactly how the weak bonds affect both the elasticity- and fracture-related mechanical properties of the chitosan composite is not clearly understood and is a subject for further study.

As noted in Section 4.1, in cases where the interaction between particle type and concentration is significant, the optimal particle concentration for each mechanical parameter differs depending on the particle type. This appears to reflect the varying degree of agglomeration by each particle type and may have to do with the degree of the proximity of particles within an agglomerate. Accordingly, from computational studies on particle–particle proximity [68], it is inferred that (A) the interphase material surrounding a particle could overlap with the interphase material from neighbouring particles, and (B) the mechanical properties of the nanoparticulate-reinforced composite could depend on the degree of the interphase-interphase overlap. It then follows that particle clustering increases appreciably at high particle concentration levels. Consequently, this leads to decreases in the E of the nanoparticulate-reinforced composites [68].

The non-linear relationship between the mechanical property of a composite and the particle concentration, and the existence of an optimal particle concentration that results in the characteristic peak value of the mechanical parameter, means that predicting the mechanical properties of these composites may not be as straightforward as we would like. As pointed out in Section 4.1, these non-linear effects are found in many particle-reinforced composite systems. For instance, polypropylene reinforced by $BaSO_4$ nanoparticles reveals an increasing σ_Y with increasing particle concentration up to 10% (w/w); thereafter a trending decrease occurs with increasing particle concentration [66]. Polyimide reinforced by SiO_2 particles reveals an increasing σ_U with particle concentration for up to 5% (w/w); thereafter σ_U decreases with increasing particle concentration [1]. Epoxy reinforced by hydrated $Al(OH)_3$ nanoparticles results in increasing G (fracture toughness in kJ/m^2) with particle concentration from 20% to 30% (w/w); thereafter a decreasing G with particle concentration was observed [71]. Nevertheless, there are exceptions, e.g., dentin composites reinforced by hydroxyapatite nanoparticles reveal a monotonically increasing (flexural) E with increase in particle concentration (the maximum particle concentration studied was 15% w/w) [72]; it remains to be seen if E also peaks at a certain particle concentration thereafter before decreasing. Recently, simple constitutive equations based on phenomenological arguments have been proposed to model these non-linear effects for fracture strength and stiffness [49]. The underlying basis of the model suggests that the initial linear increase in the magnitude of the respective mechanical property with increase in particle concentration follows the rule-of-mixture [49]. Beyond a certain particle concentration, the matrix mechanical property dominates so that the mechanical property experiences decrease in magnitude with increasing particle concentration [49]. Nevertheless, this model has to be investigated further before it can be used in practical applications.

5. Conclusions

It is shown in this study that only the fracture-related properties were sensitive to effects arising from the interaction between the particle type and concentration. Most mechanical properties are sensitive to particle type; for instance, the stiffness and yield strength of CS/POSS fibres are higher than those of CS/HA fibres. On the other hand, the yield strain, extensibility and fracture toughness of CS/POSS fibres are lower than those of CS/HA fibres. Most mechanical properties are sensitive to varying particle concentrations. For some mechanical properties, namely stiffness and yield strength, these feature a trending increase to a peak value (the optimal particle concentration) and a trending

decrease thereafter, with increasing particle concentration. For the others, namely fracture strength, strain at fracture and fracture toughness, the sensitivity is significant but no trending increase/decrease is sustained over the particle concentration range investigated here. Predictions of the reliability of the CS composite fibres reveals that CS/HA composite fibres have a more consistent (in other words, narrower spread of σ values) yield and fracture strength as compared to CS/POSS composite fibres.

Acknowledgments: The authors gratefully acknowledge the help of Shir Lin Chew with the experimental part of this work. The authors also gratefully acknowledge the initial discussions with San Hein on the setup of the wet spinning system and the synthesis process of a chitosan composite fibre.

Author Contributions: K.W. and K.L.G. conceived and designed the experiments. K.W. and K.L.G. performed the experiments; K.W., P.P., R.T.D.S. and K.L.G. analyzed the data; K.W. contributed reagents/materials/analysis tools; K.W., P.P., R.T.D.S. and K.L.G. wrote the paper.

Conflicts of Interest: The authors declare no conflict of interests

References

1. Fu, S.Y.; Feng, X.Q.; Lauke, B.; Mai, Y.W. Effects of particle size, particle/matrix interface adhesion and particle loading on mechanical properties of particulate-polymer composites. *Compos. Part B* **2008**, *39*, 933–961. [CrossRef]
2. De Silva, R.T.; Pasbakhsh, P.; Goh, K.L.; Mishnaevsky, L. 3-D computational model of poly (lactic acid)/halloysite nanocomposites: Predicting elastic properties and stress analysis. *Polymer* **2014**, *55*. [CrossRef]
3. De Silva, R.T.; Soheilmoghaddam, M.; Goh, K.L.; Wahit, M.U.; Bee, S.A.H.; Chai, S.-P.; Pasbakhsh, P. Influence of the processing methods on the properties of poly (lactic acid)/halloysite nanocomposites. *Polym. Compos.* **2016**, *37*, 861–869. [CrossRef]
4. Khor, E.; Lim, L.Y. Implantable applications of chitin and chitosan. *Biomaterials* **2003**, *24*, 2339–2349. [CrossRef]
5. Khalil, H.P.S.A.; Saurabh, C.K.; Adnan, A.S.; Fazita, M.R.N.; Syakir, M.I.; Davoudpour, Y.; Rafatullah, M.; Abdullah, C.K.; Haafiz, M.K.M.; Dungani, R. A review on chitosan-cellulose blends and nanocellulose reinforced chitosan biocomposites: Properties and their applications. *Carbohydr. Polym.* **2016**, *150*, 216–226. [CrossRef]
6. Wysokowski, M.; Bazhenov, V.V.; Tsurkan, M.V.; Galli, R.; Stelling, A.L.; Stöcker, H.; Kaiser, S.; Niederschlag, E.; Gärtner, G.; Behm, T.; et al. Isolation and identification of chitin in three-dimensional skeleton of Aplysina fistularis marine sponge. *Int. J. Biol. Macromol.* **2013**, *62*, 94–100. [CrossRef] [PubMed]
7. Wysokowski, M.; Petrenko, I.; Stelling, A.L.; Stawski, D.; Jesionowski, T.; Ehrlich, H. Poriferan chitin as a versatile template for extreme biomimetics. *Polymers* **2015**, *7*, 235–265. [CrossRef]
8. Wysokowski, M.; Materna, K.; Walter, J.; Petrenko, I.; Stelling, A.L.; Bazhenov, V.V.; Klapiszewski, Ł.; Szatkowski, T.; Lewandowska, O.; Stawski, D.; et al. Solvothermal synthesis of hydrophobic chitin-polyhedral oligomeric silsesquioxane (POSS) nanocomposites. *Int. J. Biol. Macromol.* **2015**, *78*, 224–229. [CrossRef] [PubMed]
9. Obara, K.; Ishihara, M.; Ishizuka, T.; Fujita, M. Photocrosslinkable chitosan hydrogel containing fibroblast growth factor-2 stimulates wound healing in healing-impaired db/db mice. *Biomaterials* **2003**, *24*, 3437–3444. [CrossRef]
10. Cheng, M.; Deng, J.; Yang, F.; Gong, Y.; Zhao, N.; Zhang, X. Study on physical properties and nerve cell affinity of composite films from chitosan and gelatin solutions. *Biomaterials* **2003**, *24*, 2871–2880. [CrossRef]
11. Malheiro, V.N.; Caridade, S.G.; Alves, N.M.; Mano, J.F. New poly (e-caprolactone)/chitosan blend fibers for tissue engineering applications. *Acta Biomater.* **2010**, *6*, 418–428. [CrossRef] [PubMed]
12. Alves, N.M.; Mano, J.F. Chitosan derivatives obtained by chemical modifications for biomedical and environmental applications. *Int. J. Biol. Macromol.* **2008**, *43*, 401–414. [CrossRef] [PubMed]
13. Di Martino, A.; Sittinger, M.; Risbud, M.V. Chitosan: A versatile biopolymer for orthopaedic tissue-engineering. *Biomaterials* **2005**, *26*, 5983–5990. [CrossRef] [PubMed]

14. Albanna, M.Z.; Bou-Akl, T.H.; Blowytsky, O.; Walters, H.L.; Matthew, H.W.T. Chitosan fibers with improved biological and mechanical properties for tissue engineering applications. *J. Mech. Behav. Biomed. Mater.* **2013**, *20*, 217–226. [CrossRef] [PubMed]
15. Liu, M.; Zhang, Y.; Wu, C.; Xiong, S.; Zhou, C. Chitosan/halloysite nanotubes bionanocomposites: Structure, mechanical properties and biocompatibility. *Int. J. Biol. Macromol.* **2012**, *51*, 566–575. [CrossRef] [PubMed]
16. De Silva, R.T.; Pasbakhsh, P.; Goh, K.L.; Chai, S.-P.; Ismail, H. Physico-chemical characterisation of chitosan/halloysite composite membranes. *Polym. Test.* **2013**, *32*, 265–271. [CrossRef]
17. Govindasamy, K.; Fernandopulle, C.; Pasbakhsh, P.; Goh, K.L. Synthesis and characterisation of electrospun chitosan membranes reinforced by halloysite nanotubes. *J. Mech. Med. Biol.* **2014**, *14*, 1450058. [CrossRef]
18. Goh, K.L.; Listrat, A.; Béchet, D. Hierarchical mechanics of connective tissues: Integrating insights from nano to macroscopic studies. *J. Biomed. Nanotechnol.* **2014**, *10*, 2464–2507. [CrossRef]
19. Wong, W.L.E.; Joyce, T.J.; Goh, K.L. Resolving the viscoelasticity and anisotropy dependence of the mechanical properties of skin from a porcine model. *Biomech. Model. Mechanobiol.* **2016**, *15*, 433–446. [CrossRef] [PubMed]
20. Goh, K.L.; Holmes, D.F.; Lu, H.Y.; Richardson, S.; Kadler, K.E.; Purslow, P.P.; Wess, T.J. Ageing changes in the tensile properties of tendons: Influence of collagen fibril volume. *J. Biomech. Eng.* **2008**, *130*, 21011. [CrossRef] [PubMed]
21. Goh, K.L.; Chen, Y.; Chou, S.M.; Listrat, A.; Bechet, D.; Wess, T.J.J. Effects of frozen storage temperature on the elasticity of tendons from a small murine model. *Animal* **2010**, *4*, 1613–1617. [CrossRef] [PubMed]
22. Goh, K.L.; Holmes, D.F.; Lu, Y.; Purslow, P.P.; Kadler, K.E.; Bechet, D.; Wess, T.J. Bimodal collagen fibril diameter distributions direct age-related variations in tendon resilience and resistance to rupture. *J. Appl. Physiol.* **2012**, *113*, 878–888. [CrossRef] [PubMed]
23. Yeo, Y.L.; Goh, K.L.; Kin, L.; Wang, H.J.; Listrat, A.; Bechet, D. Structure-property relationship of burn collagen reinforcing musculo-skeletal tissues. *Key Eng. Mater.* **2011**, *478*, 87–92. [CrossRef]
24. Goh, K.L.; Chen, S.Y.; Liao, K. A thermomechanical framework for reconciling the effects of ultraviolet radiation exposure time and wavelength on connective tissue elasticity. *Biomech. Model. Mechanobiol.* **2014**. [CrossRef] [PubMed]
25. Xie, J.Z.; Hein, S.; Wang, K.; Liao, K.; Goh, K.L. Influence of hydroxyapatite crystallization temperature and concentration on stress transfer in wet-spun nanohydroxyapatite-chitosan composite fibres. *Biomed. Mater.* **2008**, *3*, 2–6. [CrossRef] [PubMed]
26. Chew, S.L.; Wang, K.; Chai, S.P.; Goh, K.L. Elasticity, thermal stability and bioactivity of polyhedral oligomeric silsesquioxanes reinforced chitosan-based microfibres. *J. Mater. Sci. Mater. Med.* **2011**, *22*, 1365–1374. [CrossRef] [PubMed]
27. Blanco, I.; Abate, L.; Bottino, F.A. Synthesis and thermal properties of new dumbbell-shaped isobutyl-substituted POSSs linked by aliphatic bridges. *J. Therm. Anal. Calorim.* **2014**, *116*, 5–13. [CrossRef]
28. Guo, Y.-P.; Guan, J.-J.; Yang, J.; Wang, Y.; Zhang, C.-Q.; Ke, Q.-F. Hybrid nanostructured hydroxyapatite–chitosan composite scaffold: Bioinspired fabrication, mechanical properties and biological properties. *J. Mater. Chem. B* **2015**, *3*, 4679–4689. [CrossRef]
29. Yamaguchi, I.; Tokuchi, K.; Fukuzaki, H.; Koyama, Y.; Takakuda, K.; Monma, H.; Tanaka, J. Preparation and microstructure analysis of chitosan/hydroxyapatite nanocomposites. *J. Biomed. Mater. Res.* **2001**, *55*, 20–27. [CrossRef]
30. De Silva, R.; Pasbakhsh, P.; Qureshi, A.J.; Gibson, A.G.; Goh, K.L. Stress transfer and fracture in nanostructured particulate-reinforced chitosan biopolymer composites: Influence of interfacial shear stress and particle slenderness. *Compos. Interfaces* **2014**, *21*, 807–818. [CrossRef]
31. Peniche, C.; Solís, Y.; Davidenko, N.; García, R. Chitosan/hydroxyapatite-based composites. *Biotecnol. Apl.* **2010**, *27*, 202–210.
32. Pighinelli, L.; Kucharska, M. Properties and structure of microcrystalline chitosan and hydroxyapatite composites. *J. Biomater. Nanobiotechnol.* **2014**, *5*, 128–138. [CrossRef]
33. Wang, Z.; Hu, Q. Preparation and properties of three-dimensional hydroxyapatite/chitosan nanocomposite rods. *Biomed. Mater.* **2010**, *5*, 45007. [CrossRef] [PubMed]
34. Wang, K.; Liao, K.; Goh, K.L. How sensitive is the elasticity of hydroxyapatite-nanoparticle- reinforced chitosan composite to changes in particle concentration and crystallization temperature? *J. Funct. Biomater.* **2015**, *6*, 986–998. [CrossRef] [PubMed]

35. Tishchenko, G.; Bleha, M. Diffusion permeability of hybrid chitosan/polyhedral oligomeric silsesquioxanes (POSS) membranes to amino acids. *J. Membr. Sci.* **2005**, *248*, 45–51. [CrossRef]
36. Xu, D.; Loo, L.S.; Wang, K. Pervaporation performance of novel chitosan-POSS hybrid membranes: Effects of POSS and operating conditions. *J. Polym. Sci. Part B* **2010**, *48*, 2185–2192. [CrossRef]
37. Reno, F.; Carniato, F.; Rizzi, M.; Marchese, L.; Laus, M.; Antonioli, D.; Ren, F. POSS/gelatin-polyglutamic acid hydrogel composites: Preparation, biological and mechanical characterization. *J. Appl. Polym. Sci.* **2013**, 699–706. [CrossRef]
38. Zhang, W.; Camino, G.; Yang, R. Polymer/polyhedral oligomeric silsesquioxane (POSS) nanocomposites: An overview of fire retardance. *Prog. Polym. Sci.* **2017**, *67*, 77–125. [CrossRef]
39. Blanco, I.; Bottino, F.A.; Cicala, G.; Latteri, A.; Recca, A. Synthesis and Characterization of Differently Substituted Phenyl Hepta Isobutyl-Polyhedral Oligomeric Silsesquioxane/Polystyrene Nanocomposites. *Polym. Compos.* **2014**, *35*, 151–157. [CrossRef]
40. Andrade, R.J.; Weinrich, Z.N.; Ferreira, C.I.; Schiraldi, D.A.; Maia, J.M. Optimization of Melt Blending Process of Nylon 6-POSS: Improving mechanical properties of spun fibers. *Polym. Eng. Sci.* **2015**, *55*, 1580–1587. [CrossRef]
41. Raftopoulos, K.N.; Pielichowski, K. Segmental dynamics in hybrid polymer/POSS nanomaterials. *Prog. Polym. Sci.* **2016**, *52*, 136–187. [CrossRef]
42. Lee, S.; Park, S.; Kim, Y. Effect of the concentration of sodium acetate (SA) on crosslinking of chitosan fiber by epichlorohydrin (ECH) in a wet spinning system. *Carbohydr. Polym.* **2007**, *70*, 53–60. [CrossRef]
43. Wang, K.; Loo, L.S.; Goh, K.L. A facile method for processing lignin reinforced chitosan biopolymer microfibres: Optimising the fibre mechanical properties through lignin type and concentration. *Mater. Res. Express* **2016**, *3*. [CrossRef]
44. Weibull, W. A statistical distribution function of wide applicability. *ASME J. Appl. Mech.* **1951**, *18*, 293–297.
45. O'Brien, F.J.; Harley, B.A.; Yannas, I.V.; Gibson, L.J. The effect of pore size on cell adhesion in collagen-GAG scaffolds. *Biomaterials* **2005**, *26*, 433–441. [CrossRef] [PubMed]
46. O'Brien, F.J. Biomaterials & scaffolds for tissue engineering. *Mater. Today* **2011**, *14*, 88–95.
47. Ramshaw, J.A.M.; Werkmeister, J.A.; Dumsday, G.J. Emerging directions for biomedical materials Bioengineered collagens. *Bioengineered* **2017**, *5*, 227–233. [CrossRef] [PubMed]
48. Bhattarai, N.; Edmondson, D.; Veiseh, O.; Matsen, F.A.; Zhang, M. Electrospun chitosan-based nanofibers and their cellular compatibility. *Biomaterials* **2005**, *26*, 6176–6184. [CrossRef] [PubMed]
49. Goh, K.L. *Discontinuous-Fibre Reinforced Composites: Fundamentals of Stress Transfer and Fracture Mechanics*; Springer: London, UK, 2017. [CrossRef]
50. Sadat-Shojai, M.; Khorasani, M.-T.; Jamshidi, A. Hydrothermal processing of hydroxyapatite nanoparticles—A Taguchi experimental design approach. *J. Cryst. Growth* **2012**, *361*, 73–84. [CrossRef]
51. Sadat-Shojai, M.; Khorasani, M.-T.; Dinpanah-Khoshdargi, E.; Jamshidi, A. Synthesis methods for nanosized hydroxyapatite with diverse structures. *Acta Biomater.* **2013**, *9*, 7591–7621. [CrossRef] [PubMed]
52. Notin, L.; Viton, C.; David, L.; Alcouffe, P.; Rochas, C.; Domard, A. Morphology and mechanical properties of chitosan fibers obtained by gel-spinning: Influence of the dry-jet-stretching step and ageing. *Acta Biomater.* **2006**, *2*, 387–402. [CrossRef] [PubMed]
53. Denkba, E.B.; Seyyal, M.; Piskin, E. ImplanTable 5-fluorouracil loaded chitosan scaffolds prepared by wet spinning. *J. Membr. Sci.* **2000**, *172*, 33–38. [CrossRef]
54. Chen, Z.G.; Wang, P.W.; Wei, B.; Mo, X.M.; Cui, F.Z. Electrospun collagen–chitosan nanofiber: A biomimetic extracellular matrix for endothelial cell and smooth muscle cell. *Acta Biomater.* **2010**, *6*, 372–382. [CrossRef] [PubMed]
55. Kumar, R.; Prakash, K.H.; Cheang, P.; Khor, K.A. Temperature driven morphological changes of chemically precipitated hydroxyapatite nanoparticles. *Langmuir* **2004**, *8*, 5196–5200. [CrossRef]
56. Banerjee, A.; Bandyopadhyay, A.; Bose, S. Hydroxyapatite nanopowders: Synthesis, densification and cell–materials interaction. *Mater. Sci. Eng. C* **2007**, *27*, 729–735. [CrossRef]
57. Strachota, A.; Tishchenko, G.; Matejka, L.; Bleha, M. Chitosan–oligo(silsesquioxane) blend membranes: Preparation, morphology, and diffusion permeability. *J. Inorg. Organomet. Polym.* **2002**, *11*, 165–182. [CrossRef]
58. Kopesky, E.T.; McKinley, G.H.; Cohen, R.E. Toughened poly(methyl methacrylate) nanocomposites by incorporating polyhedral oligomeric silsesquioxanes. *Polymer* **2006**, *47*, 299–309. [CrossRef]

59. Ayandele, E.; Sarkar, B.; Alexandridis, P. Polyhedral oligomeric silsesquioxane (POSS)-containing polymer nanocomosites. *Nanomaterials* **2012**, *2*, 445–475. [CrossRef] [PubMed]
60. Motskin, M.; Wright, D.M.; Muller, K.; Kyle, N.; Gard, T.G.; Porter, A.E.; Skepper, J.N. Biomaterials hydroxyapatite nano and microparticles: Correlation of particle properties with cytotoxicity and biostability. *Biomaterials* **2009**, *30*, 3307–3317. [CrossRef] [PubMed]
61. Goh, K.L.; Aspden, R.M.; Mathias, K.J.; Hukins, D.W.L. Finite-element analysis of the effect of material properties and fibre shape on stresses in an elastic fibre embedded in an elastic matrix in a fibre-composite material. *Proc. R. Soc. Lond. A* **2004**, 2339–2352. [CrossRef]
62. Goh, K.L.; Aspden, R.M.; Mathias, K.J.; Hukins, D.W.L. Effect of fibre shape on the stresses within fibres in fibre-reinforced composite materials. *Proc. R. Soc. Lond. A* **1999**, *455*, 3351–3361. [CrossRef]
63. Goh, K.L.; Aspden, R.M.; Hukins, D.W.L. Review: Finite element analysis of stress transfer in short-fibre composite materials. *Compos. Sci. Technol.* **2004**, *64*, 1091–1100. [CrossRef]
64. Fu, S.; Xu, G.; Mai, Y. On the elastic modulus of hybrid particle/short-fiber/polymer composites. *Compos. Part B* **2002**, *33*, 291–299. [CrossRef]
65. Venkateshwaran, N.; Elayaperumal, A.; Sathiya, G.K. Prediction of tensile properties of hybrid-natural fiber composites. *Compos. Part B* **2012**, *43*, 793–796. [CrossRef]
66. Wang, K.; Wu, J.; Ye, L.; Zeng, H. Mechanical properties and toughening mechanisms of polypropylene/barium sulfate composites. *Compos. Part A* **2003**, *34*, 1199–1205. [CrossRef]
67. Estili, M.; Sakka, Y. Recent advances in understanding the reinforcing ability and mechanism of carbon nanotubes in ceramic matrix composites. *Sci. Technol. Adv. Mater.* **2014**, *15*, 64902. [CrossRef] [PubMed]
68. Wang, H.W.; Zhou, H.W.; Peng, R.D.; Mishnaevsky, L. Nanoreinforced polymer composites: 3D FEM modeling with effective interface concept. *Compos. Sci. Technol.* **2011**, *71*, 980–988. [CrossRef]
69. Aranaz, I.; Martínez-Campos, E.; Moreno-Vicente, C.; Civantos, A.; García-Arguelles, S.; del Monte, F. Macroporous calcium phosphate/chitosan composites prepared via unidirectional ice segregation and subsequent freeze-drying. *Materials* **2017**, *10*, 516. [CrossRef] [PubMed]
70. Irvine, S.A.; Venkatraman, S.S. Bioprinting and differentiation of stem cells. *Molecules* **2016**, *21*, 1188. [CrossRef] [PubMed]
71. Lange, F.F.; Radford, K.C. Fracture energy of an epoxy composite system. *J. Mater. Sci.* **1971**, *6*, 1197–1203. [CrossRef]
72. Sadat-Shojai, M.; Atai, M.; Nodehi, A.; Khanlar, L.N. Hydroxyapatite nanorods as novel fillers for improving the properties of dental adhesives: Synthesis and application. *Dent. Mater.* **2010**, *26*, 471–482. [CrossRef] [PubMed]